ORIGINAL PAPER

The Adaptive Delaunay Tessellation: a neighborhood covering meshing technique

**Alexandru Constantiniu · Paul Steinmann ·
Tom Bobach · Gerald Farin · Georg Umlauf**

Abstract In this paper we propose an unstructured hybrid tessellation of a scattered point set that minimally covers the proximal space around each point. The mesh is automatically obtained in a bounded period of time by transforming an initial Delaunay tessellation. Novel types of polygonal interpolants are used for interpolation applications and the geometric qualities of the elements make them also useful for discretization schemes. The approach proves to be superior to classical Delaunay one in a finite element context.

Keywords Adaptive Delaunay Tessellation · Polygonal interpolation · Generalized barycentric coordinates · Scattered data interpolation · Polygonal finite elements

1 Introduction

Finite elements simulations of static or transient large deformation processes involve remeshing as a necessary step for

A. Constantiniu (✉) · P. Steinmann
University of Erlangen-Nuremberg,
Institute of Applied Mechanics, Egerlandstrasse 5,
91058 Erlangen, Germany
e-mail: constantiniu@ltm.uni-erlangen.de

P. Steinmann
e-mail: steinmann@ltm.uni-erlangen.de

T. Bobach · G. Umlauf
Department of Computer Sciences, University of Kaiserslautern,
Gottlieb-Daimler-Strasse, 67653 Kaiserslautern, Germany
e-mail: bobach@informatik.uni-kl.de

G. Umlauf
e-mail: umlauf@informatik.uni-kl.de

G. Farin
Department of Computer Science and Engineering,
Arizona State University, Tempe, AZ 85287-8809, USA
e-mail: farin@asu.edu

obtaining efficient solutions. Despite several mesh-free alternatives developed in the last decade, the issue remains an open one. Ideally, the period of time needed to generate an acceptable mesh or to evaluate the nodal connectivities should be bounded and linear with the number of nodes. Several mesh-free or mesh-dependent schemes, including the classical FEM do not satisfy this criterion.

Yet, proximal space partitioning concepts like Voronoi diagrams allow us to quickly tessellate domains using clouds of points with no given connectivities between them. Furthermore, due to the advancements in the construction of polygonal interpolants [18] we are nowadays no longer bound to use simple geometrical elements for finite element meshes. Irregular polygons can provide greater flexibility in dealing with arbitrary geometries and have less sensitivity to lock under volume-preserving deformation states, among other benefits [19].

In this paper we present a novel polygonal meshing technique for scattered point distributions. The connectivity is computed in a bounded period of time and the elements are minimally covering the proximal space around each point. Recently developed generalized barycentric coordinates can be used for interpolating inside the ADT polygons and nodal integration schemes can be conveniently applied over the Voronoi cells in Galerkin method applications. The proposed scheme shows some pertinent advantages when used as a polygonal finite element meshing technique.

2 The proximal neighborhood of a point

A favorite concept in todays computational geometry area, the proximal or nearest-neighborhood has firstly been contemplated by Decartes more than three centuries ago [6]. Subsequently Dirichlet studied it in early 1850 in two and three

dimensions [7] and Voronoi generalized his work in 1908 into higher multidimensional space [20]. The intrinsic potential of Voronoi diagrams lies in their structural properties, in the existence of efficient algorithms for their construction and in their adaptability [1].

The dual concept of Delaunay tessellation was introduced in early 1934 [5] via an empty circumcircle criterion. Among all possible triangulations of a two-dimensional scattered point set the Delaunay one maximizes the minimum angle and minimizes the largest circumcircle. These basic qualities, together with the pioneering algorithms developed by Lawson in 1977 [11] and Watson in 1981 [22], made Delaunay meshing one of the most attractive and popular triangle meshing techniques available today [13].

Based on the concept of second order Voronoi sites, Sibson presented in 1980 his well known natural neighbour interpolation [15,16]. In 1995 Sambridge et al. developed a new weighted residual method for solving PDE's called the Natural Element Method (NEM) [12] by deriving analytical expressions for the spatial derivatives of Sibson's interpolant in terms of function values at the nodes. NEM was firstly applied in solid mechanics in 1998 by the inspiring thesis of Sukumar [17]. The obvious advantages of natural neighbor interpolation schemes have boosted their popularity in the recent years.

2.1 Delaunay meshing issues

Unfortunately, the Delaunay criterion doesn't necessarily lead to a tessellation that fits all purposes equally well. Firstly the tessellation is unique only if adjacent elements are not made of co-circular points. Secondly there is no guarantee that all Delaunay simplices have favorable geometrical qualities, especially in 3D where both max-min angle and min-max circumcircle properties are not valid.

The element quality issue is an ill posed problem which, depending on specific applications, can have contradictory solutions. Yet it strongly influences the condition number of the stiffness matrix and the numerical accuracy of an approximation scheme [14]. As recently proved, both small and large angles can have strong negative effects. The non-uniqueness problem has seen numerous solutions in the last years, among them deleting or inserting some points, perturbing their positions or using construction rules like the one based on two preferred directions proposed very recently by Dyken et al. [8].

Although an adjustment of the initial nodal distribution can solve these former issues, there are cases where this distribution is a priori given and should not be changed. A pioneering solution was recently proposed by Calvo, Idelsohn and Oñate [3]. Given an arbitrary point distribution, an Extended Delaunay Tessellation (EDT) is created by merging each set of almost co-circular points into a single polygon.

This tessellation is a unique mixture of Delaunay triangles and polygons defined by points lying on the same or nearby Delaunay circumcircles. Conveniently, the majority of elements in an EDT are still Delaunay simplices, allowing the use of linear shape functions over them. The remaining n-gons are convex and allow the application of non-Sibsonian shape functions [2]. The EDT approach solves the degenerated cases encountered in a classical Delaunay scheme and renderes a unique mesh.

Tessellating a scattered nodal distribution in an optimal way is far from being a closed problem and it is our view that simplices should not be seen as the single building blocks, especially in a proximal neighborhood context.

3 The Adaptive Delaunay Tessellation

We build our tessellation with two purposes in mind. First, the mesh should be unique, computed in a bounded period of time, with no manual modifications and without any perturbation or deletion of the given nodes. Second, the elements should have good geometrical qualities as desired in numerical approximation schemes and should minimally cover the proximal space around the nodes. This later requirement makes sense if we want the elements to be optimally adapted to a scattered nodal distribution.

The geometrical entity that perfectly records the proximity to a set of points is the Voronoi diagram. Contrary to what is generally assumed, the Delaunay tessellation is not a "real" dual of the Voronoi diagram for two reasons: first it is not unique and secondly the Delaunay simplices connected to one point do not necessary cover its corresponding Voronoi tile. In other words, a Delaunay tessellation will better represent the neighbors of a point than the proximal space around it. The dual construction that satisfies both previous requirements are the covering spheres, better known as empty circumcircles in the literature.

We will show that starting from Delaunay simplices we can obtain a minimal polygonal covering of the Voronoi cells by tracing their corresponding circumcenters and merging them into superior quality polygons. The obtained tessellation is unique and optimally adapted to the initial distribution. Further benefits will be highlighted in the following paragraphs.

3.1 Constructing the ADT

We propose the following construction to render a Delaunay triangulation into a unique tessellation in $\mathbf{R}^2$, although a similar approach also applies to higher dimensions, as will be demonstrated in a forthcomming work.

Definition 1 (Adaptive Delaunay Tessellation) Let DT $(\mathbf{P}) = (E_{\mathrm{DT}}, F_{\mathrm{DT}})$ be a Delaunay triangulation of $\mathbf{P} \subset \mathbf{R}^2$ with edges E_{DT} and triangular faces F_{DT}. The boundary of the convex hull of $\mathbf{P}$ is denoted by $\partial \mathscr{C}(\mathbf{P})$. An angle greater or equal to $\pi/2$ is considered obtuse, and so is a triangle having an obtuse angle. If a triangle f is obtuse, $e_f^> \in f$ denotes its longest edge, which is always opposite to its obtuse angle, and we call $e_f^>$ an obtuse edge.

Let

$$E' := \{e_f^> \mid f \in F_{\mathrm{DT}} \wedge e_f^> \not\subset \partial \mathscr{C}(\mathbf{P})\}$$

be the set of all obtuse edges that are not on the boundary of the convex hull of $\mathbf{P}$, and

$$E_{\mathrm{ADT}} := E_{\mathrm{DT}} \setminus E'$$

be a set of edges.

The unique tessellation $(E_{\mathrm{ADT}}, F_{\mathrm{ADT}})$ is called *Adaptive Delaunay Tessellation* (ADT) of $\mathbf{P}$.

The ADT is constructed from the Delaunay triangulation by iterating over its triangles. Since a 2D Delaunay Triangulation can be constructed in $O(n \log n)$ complexity, the linear overhead from the ADT construction is negligible. This also holds for dynamic updates coming from local retriangulations like in Delaunay repair approaches.

3.2 Properties of the ADT

The ADT offers some properties distinct from those of the Delaunay triangulation. The ADT is unique, even if the Delaunay triangulation is not. As long as the Delaunay triangulation contains no ambiguous cases, this is obvious by construction. Otherwise, all ambiguous edges are obtuse edges and will be removed, making the ADT unique again. In Fig. 1a, consider the triangles formed by $\{P, N_2, N_3, N_4\}$, and $\{P, N_5, N_6, N_7\}$ with circumcenters V_2 and V_4, respectively: the ambiguous edges $(N_3, P)/(N_2, N_4)$ and $(N_6, P)/(N_5, N_7)$ are removed, as shown in Fig. 1b. Special care, i.e. epsilon thresholding, must be taken in case the circumcenter is located on an ambiguous Delaunay edge. Since both triangles adjacent to that edge are rectangular, round-off errors might classify both as non-obtuse, thus preventing the removal of the ambiguous edge.

Furthermore, the ADT tessellation is optimal in the sense that no interior simplex has an angle greater than $\pi/2$, and the polygonal elements have as rounded shapes as possible for the given nodal distribution. Consider Fig. 2a, displaying the setting from Fig. 1a with deliberately changed positions for nodes A_1, A_2 and N_6.

As expected, the initial Delaunay triangulation does not satisfy the goal of having as round elements as possible. Slightly altering the node positions or merging the co-circular ones into polygons will not help either. In the ADT, all the
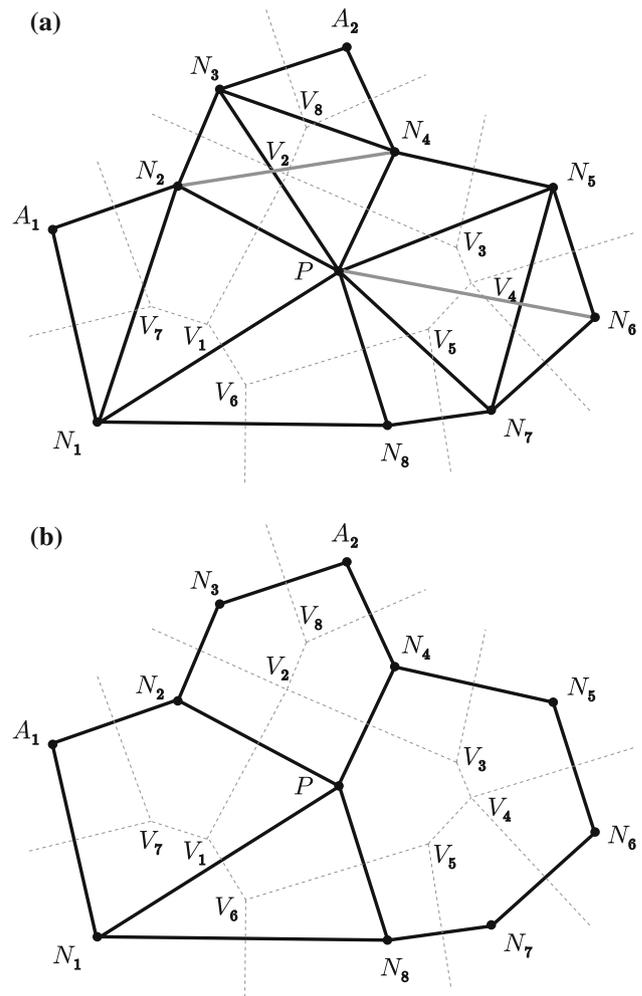
Fig. 1 (**a**) Part of a Delaunay triangulation, (**b**) Adaptive Delaunay Tessellation of (**a**). The *dotted lines* denote the Voronoi diagram, P is the central point, N its natural neighbors, A other points and V vertices in the Voronoi diagram around P

skinny, obtuse triangles are merged with others to form polygons with a rounder shape. Note that this does not necessarily eliminate skinny, isoscele triangles. We consider this alternative optimal for the given nodal distribution.

Given the construction, it is very likely that all the mentioned properties of an Adaptive Delaunay Tessellation are valid in higher dimensions, too. In 3D, many badly shaped elements can appear in a normal Delaunay tetrahedralization. Some of them are considered acceptable drawbacks, others have to be eliminated due to the errors induced. The fact that most elements are non-obtuse in an ADT makes it increasingly important in these cases.

The construction of the ADT yields no disconnected elements, which can be shown based on the fact that it starts with a Delaunay triangulation.

Finally, a point's Voronoi cell is completely covered by its adjacent ADT elements, which is not true for a Delaunay
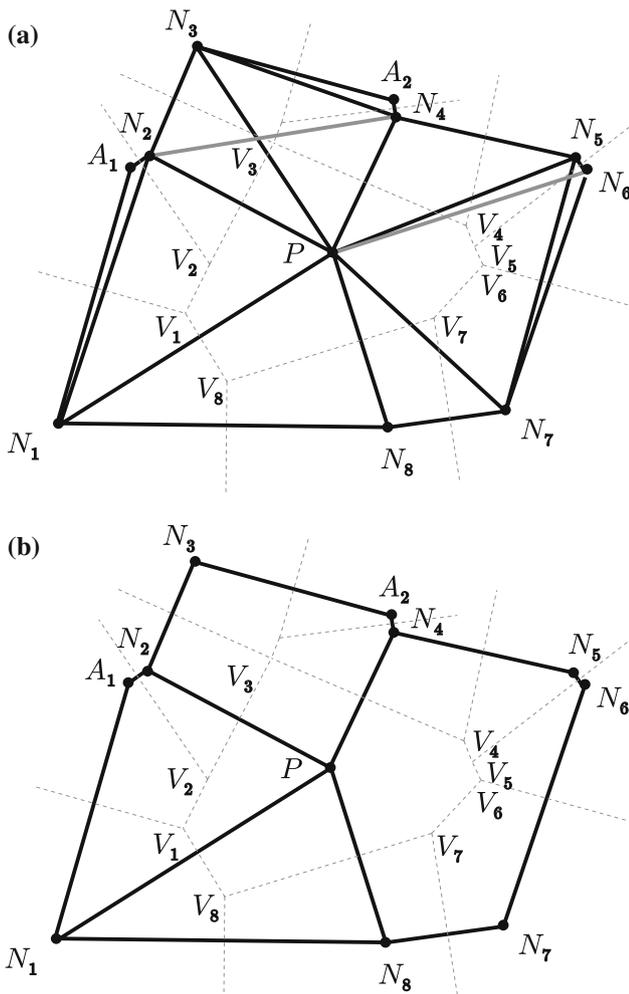
(a)

(b)

Fig. 2 The setting from Fig. 1 with deliberately changed node positions

Fig. 3 Intersection with Voronoi cell

Fig. 4b. The ADT, however, copes with the less uniform point distribution by generating more well-shaped polygons.

4 An element condition number for arbitrary polygons

In mesh-based discretization methods the sizes and shapes of elements have a direct influence on the accuracy of the numerical results. Even a small number of badly shaped elements can already compromise the whole discretization process. For the most common types of elements used today, error bounds and quality measures have been provided. Still, shape measures for general polygonal elements are almost inexistent.

In the sequel we will have to compare the shapes of simple[1] polygons with different numbers of vertices. Traditional measures such as maximum or minimum angle are not sufficient for this task so we will employ an alternate shape measure. We will assume that all polygons under consideration have their centroids at the origin.

A measure $s(\mathbf{P})$ for the shape of a polygon $\mathbf{P} = (P_1, \ldots, P_n)$ should have the following properties:

1. $s(\mathbf{P})$ is lowest for regular polygons.
2. $s(\mathbf{P})$ is a smooth function of $\mathbf{P}$'s vertices.
3. $s(\mathbf{P})$ does not change if $\mathbf{P}$ is scaled uniformly in x and y.
4. $s(\mathbf{P})$ does not change if $\mathbf{P}$ is rotated around the origin, i.e., $\mathbf{P}$'s centroid.

We now propose a shape measure meeting the above objectives. Let $\mathbf{P}$ be a polygon having n vertices P_i. Then $\mathbf{P}$ may

triangulation. To illustrate this property we look at an ADT tessellation of a point P in Fig. 3. We mark the midpoints of the ADT edges adjacent to P by $M_1, \ldots, M_4$, which are just the intersections of the ADT edges with the Voronoi cell boundary for P. If we now follow the Voronoi cell boundary, each segment is either contained in an ADT element or it perpendicularly intersects an ADT edge adjacent to P.

We need to mention that an ADT can admit non-convex polygons, which requires extra care to be taken and narrows the spectrum of available shape functions over ADT elements. We have dealt with non-convex polygons by using mean value coordinates [9].

We illustrate the properties of the ADT by comparing it to the Delaunay triangulation for two slightly different point sets as shown in a simple example in Fig. 4a. In contrast to the Delaunay triangles the ADT polygons have been shaded (Fig. 4c). Note the slightly less uniform distribution in the right point set, leading to more badly shaped triangles in
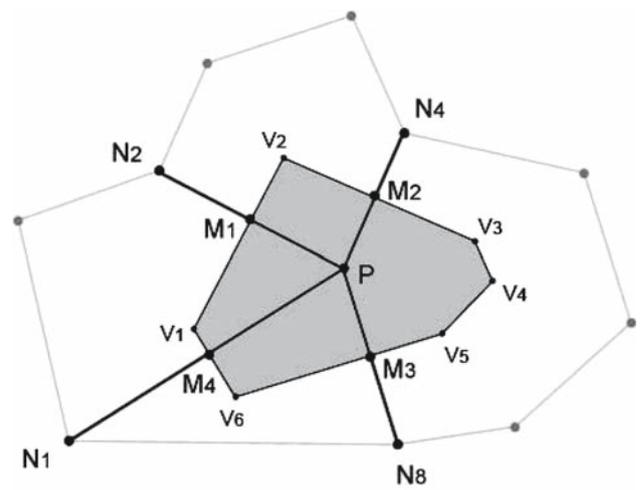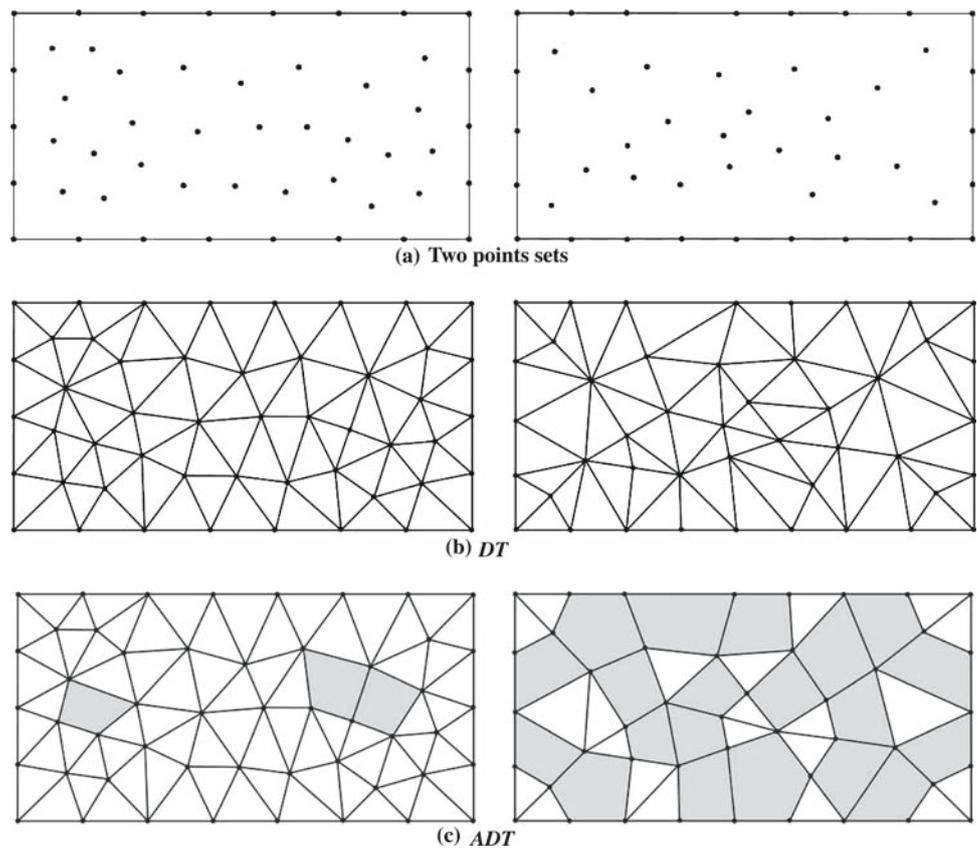
---

[1] A polygon is simple if no two of its edges intersect.

Fig. 4 Delaunay triangulation (DT) and Adaptive Delaunay Tessellation (ADT) of two slightly different scattered point sets

(a) Two points sets

(b) *DT*

(c) *ADT*

be written as a $1 \times n$ matrix

$$\mathbf{P} = [P_1, \ldots, P_n].$$

Let

$$A = \mathbf{P}^{\mathrm{T}} \cdot \mathbf{P}$$

be the *correlation matrix* of $\mathbf{P}$. It is used in the Principal Components Analysis (PCA) of point sets. The PCA finds a best fitting ellipse to the point set. Its axes are the (normalized) eigenvectors of A; the lengths of the axes are given by the square roots of its (real and positive) eigenvalues σ_1 and σ_2. The ratio of these lengths (largest value σ_1 divided by smallest value σ_2) is known as $\mathbf{P}$'s condition number cond($\mathbf{P}$). If $\mathbf{P}$ is a regular polygon, then cond($\mathbf{P}$) $= 1$. In all other cases, cond($\mathbf{P}$) ≥ 1.

We propose to use cond($\mathbf{P}$) as the shape measure for the polygon $\mathbf{P}$. The proposed shape measure is an analytic function of $\mathbf{P}$'s vertices; this follows since σ_1 and σ_2 are analytic functions of A's elements.

cond($\mathbf{P}$) is infinite for degenerate polygons (meaning all of $\mathbf{P}$'s vertices are on one straight line). A general $\mathbf{P}$ has rank 2, whereas a degenerate one only has rank 1, resulting in A being singular. Thus, cond($\mathbf{P}$) $= \infty$.

cond($\mathbf{P}$) does not change if $\mathbf{P}$ is scaled uniformly in x and y. If $\mathbf{P}$ is scaled by a factor c, then so is A and hence its eigenvalues. Thus their ratio remains constant.

cond($\mathbf{P}$) does not change if $\mathbf{P}$ is rotated around the origin, i.e., $\mathbf{P}$'s centroid. If $\mathbf{P}$ is rotated by a matrix R, the matrix A is changed to $A' = \mathbf{P}^{\mathrm{T}} R^{\mathrm{T}} R \mathbf{P}$, hence $A' = A$.

A drawback of our shape measure is that it is "blind" to vertex ordering. But since our polygons are simple, this is not considered harmful.

5 Quality measures

We have proposed a new polygonal tessellation of a point cloud, and we claim it performs better than other schemes since it bears an improved condition number and has a minimum coverage of the Voronoi cells in comparison to the Delaunay triangulation. Although polygonal approaches provide more flexibility, our method can also produce non-convex polygons. We therefore present the results of statistical analysis of the ADT's properties to examine the development of condition number, number and valence of polygons, and number of non-convex polygons depending on several parameters of the point cloud.

The basic setting consists of a regular grid of 50×50 points distributed over the unit square, which we distort by a normal distributed random variable in x and y with a variance of 0.2 and a radius of 0.025. The coordinates of points outside the unit square after the random term was added are clamped. In order to prevent too degenerate cases, we removed all points that were closer to another point than the minimum allowed distance of 30% of the grid size.

The following is a statistical analysis of some of the ADT properties in the following scenarios:

1. variable resolution of points (ratio boundary vs. interior),
2. variable randomness in the distribution of points,
3. variable linear deformation of an initial point set.

Each of those scenarios has been analyzed in a sequence of feasible settings, repeating each concrete setup ten times on different random points to improve statistical significance. The charts display the arithmetic mean of ten independent runs for a given setup.

Each time the ADT is generated we extract

1. the mean condition number of the elements,
2. the percentage of non-convex polygons,
3. the histogram of polygon valences (how many 4-gons, 5-gons, etc.).

5.1 Variable resolution

In this scenario we compare the mean condition numbers at different resolutions in order to examine the influence of the ratio between boundary and inner elements on the mean condition number. The results shown in Fig. 5 confirm the hypothesis that only for very small resolutions the worse shape of the boundary elements has significant influence on the mean condition number, yet this effect is far less visible for the ADT, which comes with better results than the DT.

5.2 Variable randomness

We want to evaluate the ADT for point sets exposing different levels of randomness. We therefore vary the Gauss radius $r \in [0.0, 0.0471]$, which results in the corresponding tessellations shown in Fig. 6 from left to right.

As expected, for $r = 0$, DT($\mathbf{P}$) consists entirely of ambiguous settings that are merged into quadrilaterals in ADT($\mathbf{P}$). While r grows, the triangles in DT($\mathbf{P}$) get closer to equilateral at first with a moderate distortion, but become increasingly ill-shaped for larger randomness. This can be verified with the condition numbers in Fig. 7a. The chart only displays the condition numbers of inner elements, as the condition
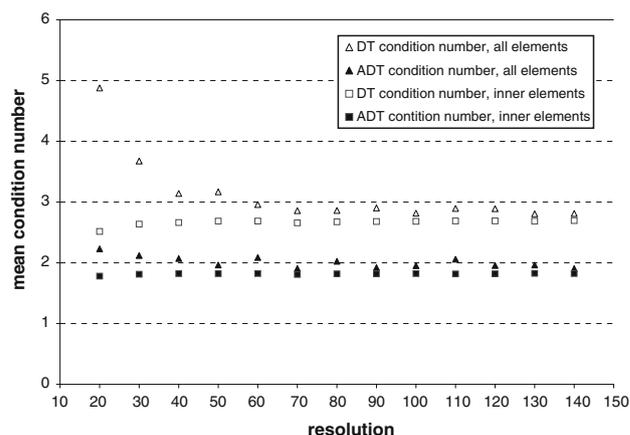
Fig. 5 Comparison of condition numbers for DT($\mathbf{P}$) and ADT($\mathbf{P}$) considering variable resolutions. This diagram illustrates the influence of boundary elements, which usually retain a bad condition number. If the resolution increases, the ratio between inner and boundary elements changes in favor of the mean condition number

numbers for close-to degenerate Delaunay triangles on the convex hull are arbitrary close to infinity. Figure 7b displays the development of non-convex elements, the results of all 10 runs plotted on top of each other to give an impression of the deviation. We consider all elements, and the contribution of non-convex elements seen in the range $r \in [0, 0.4]$ result from non-convex boundary elements. Interestingly, the number of non-convex elements seems to stay constant around 5 to 6%, although with a higher deviation.

We compare the mean condition numbers at different resolutions in order to examine the influence of the ratio between boundary and inner elements on the mean condition number. The results shown in Fig. 7 confirm the hypothesis that only for very small resolutions the worse shape of the boundary elements has significant influence on the mean condition number, yet this effect is far less visible for the ADT, which again comes with better results than the DT.

5.3 Variable linear deformation

Since ADT($\mathbf{P}$) and DT($\mathbf{P}$) are implicitly defined by $\mathbf{P}$, they are naturally suited to tessellate deforming geometries. We analyze the development of the condition number under a continuous deformation of $\mathbf{P}$, which we choose to be a horizontal scaling ranging from $s = 1$ to 3, the setting for $s = 1$ and 2 shown in Fig. 8.

We have noticed one setting with exceptionally high mean condition numbers for DT($\mathbf{P}$), the development of the mean condition number depicted in Fig. 9. In contrast to the remaining nine test cases, the mean condition number for DT($\mathbf{P}$) was constantly increasing, while it remained constantly low for ADT($\mathbf{P}$) (Fig. 9).
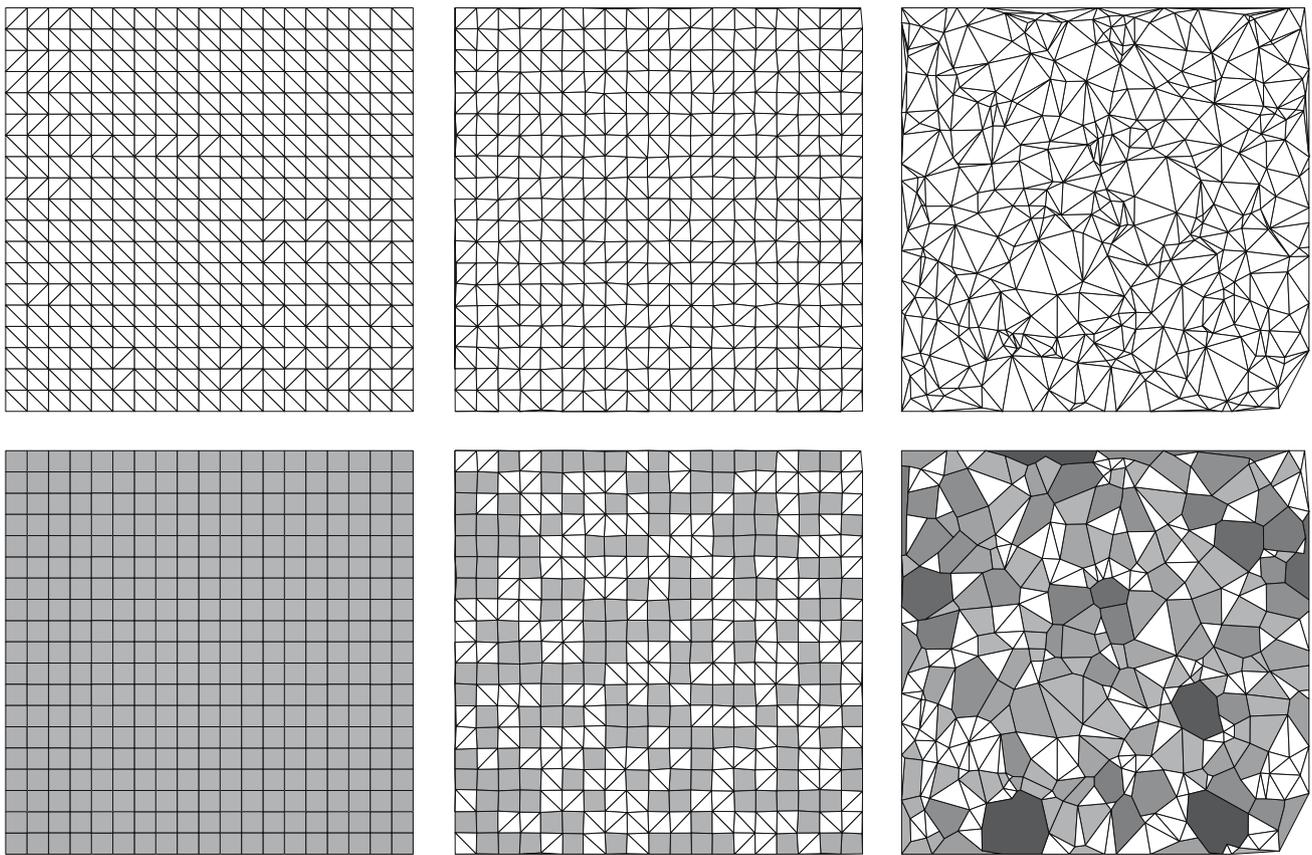
Fig. 6 DT(**P**) (*upper row*) and ADT(**P**) (*lower row*) for a Gauss radius of (**a**) $r = 0.0$, (**b**) $r = 0.00119$, and (**c**) $r = 0.0471$

5.4 Statistics summary

We found that the average condition number of the ADT is in general significantly lower than that of the Delaunay triangulation. When looking at point clouds with a different amount of randomness and different minimum distance for the nearest points, the ADT exhibits less variation. The mean condition number of an ADT settles between 1.7 and 2.0 while for a Delaunay triangulation it is usually between 2.5 and 2.7.

While a Delaunay triangulation always consists of triangles, an ADT can contain polygons of higher valence. In general, the more organized and uniform the point cloud, the lower the valence of polygons in the ADT. For sufficiently large point clouds, the element distribution in the ADT in all our test runs looks as in the table presented in Fig. 10.

The occurence of non-convex elements in the ADT is certainly a drawback. However, for uniformly ordered point sets there are no non-convex polygons and for increasingly random point distributions they never exceeded seven percent of the total number of elements.

Last but not least, boundary elements play a special role in that they can retain the bad shapes of the Delaunay triangles, since outside the convex hull there are no more triangles to merge. If boundary triangles are merged into ADT elements the resulting condition number improves, but non-convex elements are created more often than in the interior. Badly shaped triangles are a common problem in Delaunay triangulations and a further improved ADT approach can be a step forward in dealing with it.

6 Polygonal interpolants based on generalized barycentric coordinates

An ADT tessellation cannot be used in a finite elements frame without appropriate shape functions over its elements. Generalized barycentric coordinates for irregular polygons directly correspond to shape functions and were intensively studied in the last decade due to their large field of applicability.

For the present work we have used a form of rational barycentric coordinates for higher dimensions recently proposed by Warren et al. [21]. For a d-dimensional polytope **P**, given by the convex hull of its n vertices $v_n(\mathbf{P})$, each rational coordinate function per vertex $\{b_v / v \in v_n(\mathbf{P})\}$ satisfies the defining properties of barycentric coordinates
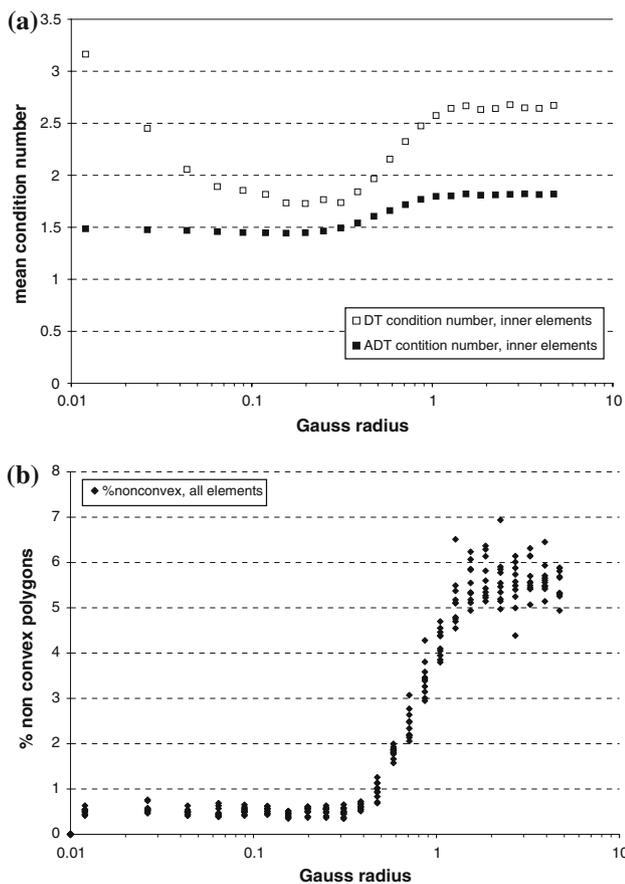
Fig. 7 (a) Comparison of the mean condition number of the DT and the ADT for a variable Gauss radius expressing a variable order of randomness—note the more or less stable behavior after some point, (b) percentage of non-convex polygons, all ten results for one value of the gauss radius displayed to show the variance. Again there appears some stabilization above some point

non-negativity $b_v(\mathbf{x}) \geq 0$ $\forall \mathbf{x} \in \mathbf{P}$,

partition of unity $\sum_{v \in v_n(\mathbf{P})} b_v(\mathbf{x}) = 1$ $\forall \mathbf{x} \in \mathbf{P}$,

linear precision $\sum_{v \in v_n(\mathbf{P})} L(v) b_v(\mathbf{x}) = L(\mathbf{x})$ $\forall \mathbf{x} \in \mathbf{P}$,

where L(**x**) is a linear function.

Furthermore, they satisfy the auxiliary properties of smoothness, tensor product and face restriction [21]. The coordinates reduce to bilinear ones for a rectangle and to linear ones on the edges of a polygon.

For simplicity we describe the planar case of a polygon **P**. We note with $d = 2$ the space dimension, with $v_n(\mathbf{P})$ the polygon's vertices and with **x** an inside point. Since each edge of **P** is defining a halfplane, the convex n-gon can be written as the intersection of n-halfplanes. Hence, we can define it as the solution of a matrix inequality

$$N\mathbf{x} \leq \mathbf{c}.$$

where $N \in \mathrm{Mat}(n \times d)$, $\mathbf{x} = [x_1, x_2]^T$ and $\mathbf{c} = [c_1, \ldots, c_n]^T$ is a column vector of length n. We assign in clockwise order

an index to each edge of the polygon, corresponding to the equation $N_i \mathbf{x} = \mathbf{c}_i$, where N_i is the ith row of N. Since each vertex is the intersection of two edges, we build an index set σ for each vertex containing the two corresponding indices. For each index set a $d \times d$ submatrix of N is formed by the corresponding rows, denoted N_σ. For every vertex, the weight functions are defined as:

$$w_\sigma(\mathbf{x}) = \frac{|\mathrm{Det}(N_\sigma)|}{n_\sigma(\mathbf{x})}$$

with $n_\sigma(\mathbf{x}) = \prod_{i \in \sigma} [\mathbf{c}_i - N_i \mathbf{x}]$ a product of d linear functions. As geometrical meaning, the numerator corresponds to the area of the parallelogram formed by the outward normals associated with the two adjacent edges of the vertex and the denominator is the product of the distances from **x** to these edges. The barycentric coordinates $b_\sigma(\mathbf{x})$ are obtained by normalizing each weight by the sum of all weights defined in the polygon.

We exemplify for the pentagon case in Fig. 11.

The edges are numbered clockwise and each vertex is identified by an index set representing the two corresponding incident edges. The outward normals and the perpendiculars from an inside point **x** to the polygon's edges have been drawn. For vertex coordinates $V_{\{5,1\}} = (-1, 1)$, $V_{\{1,2\}} = (0, 2)$, $V_{\{2,3\}} = (1, 2)$, $V_{\{3,4\}} = (1, 0.5)$, $V_{\{4,5\}} = (0, 0)$ the matrix inequality has the form

$$\begin{bmatrix} -1 & 1 \\ 0 & 1 \\ 1 & 0 \\ 0.5 & -1 \\ -1 & -1 \end{bmatrix} \begin{bmatrix} x_1 \\ x_2 \end{bmatrix} \leq \begin{bmatrix} 2 \\ 2 \\ 1 \\ 0 \\ 0 \end{bmatrix}.$$

Corresponding to each vertex the weights are

$$w_{\{5,1\}}(\mathbf{x}) = \frac{2}{[2 + x_1 - x_2][x_1 + x_2]},$$

$$w_{\{1,2\}}(\mathbf{x}) = \frac{1}{[2 - x_2][2 + x_1 - x_2]},$$

$$w_{\{2,3\}}(\mathbf{x}) = \frac{1}{[1 - x_1][2 - x_2]},$$

$$w_{\{3,4\}}(\mathbf{x}) = \frac{1}{[-0.5x_1 + x_2][1 - x_1]},$$

$$w_{\{4,5\}}(\mathbf{x}) = \frac{1.5}{[x_1 + x_2][-0.5x_1 + x_2]}.$$

As expected, the coordinates are rational and of minimum degree. They are simple to evaluate and they reduce to conventional barycentric coordinates in the case of simplices. The functions are smooth in any point **x** inside the elements and linear on the edges. In Fig. 12 we draw the barycentric coordinate functions for the point of interest P from the ADT case presented earlier in Fig. 1.

Fig. 8 DT(**P**) (*upper row*) and ADT(**P**) (*lower row*) for a horizontal scaling of the random point cloud by 1 and 2, resp
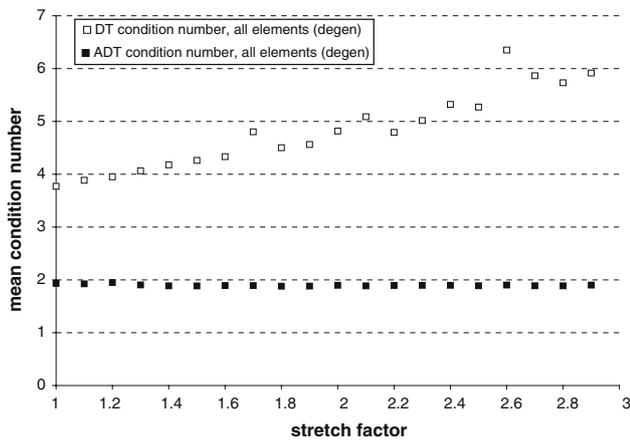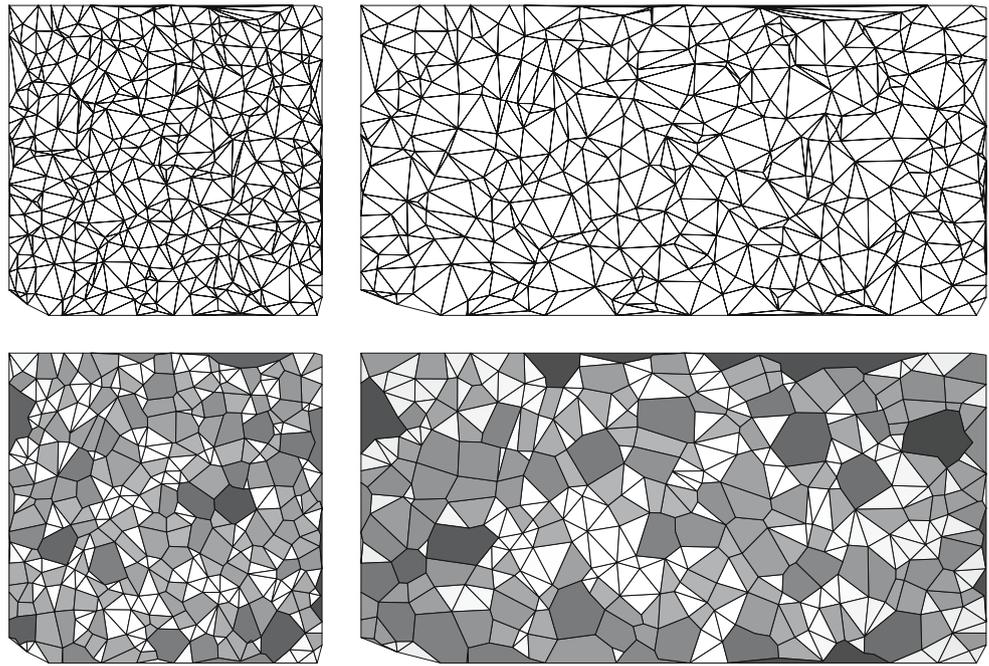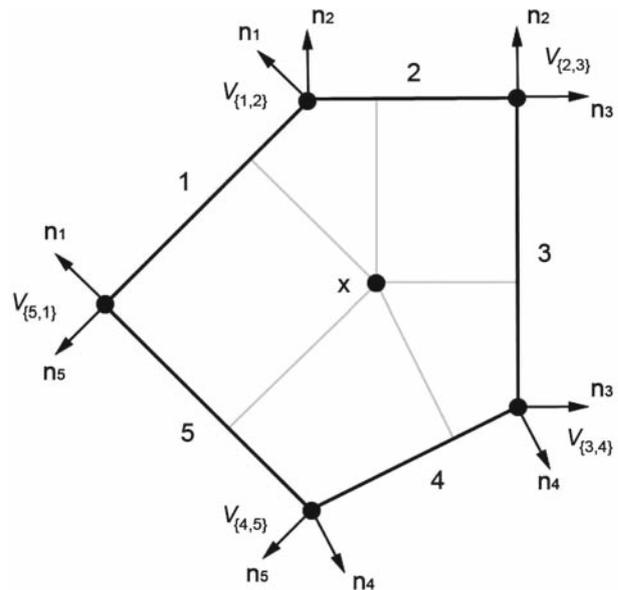

Fig. 9 Comparison of mean condition numbers of DT(**P**) and ADT(**P**) for an increasing horizontal stretch of **P** from $s = 1$ to 3

valence	3	4	5	6	...
polygons	55%	20%	10%	5%	...

Fig. 10 Distribution of element valences in large, random point clouds

Fig. 11 Irregular pentagon

The former explicit construction retains its properties in arbitrary dimensions. Yet, Warren's coordinates are less robust against obtuse angles and non-convex *n*-gons. Therefore we are considering the use of other generalized barycentric coordinates as an open choice. A good alternative option for both convex and non-convex polygonal elements are the recently proposed mean value coordinates [9].
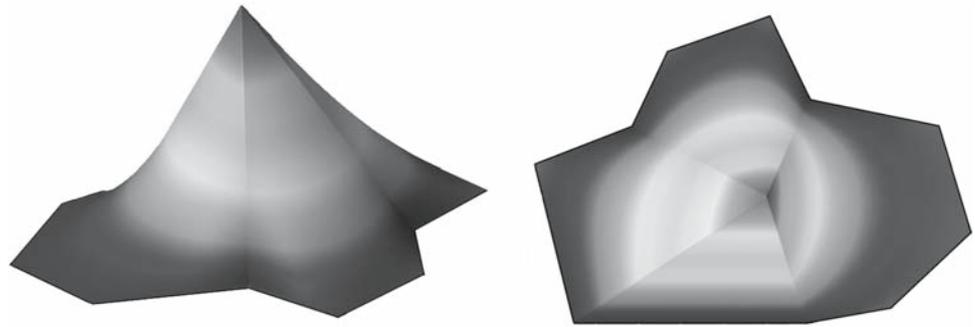
These are defined as

$$\lambda_i = \frac{w_i}{\sum_{j=1}^{k} w_j}, \qquad w_i = \frac{\tan(\alpha_{i-1}/2) + \tan(\alpha_i/2)}{\|v_i - v_0\|^2},$$

and provide convex local coordinates with linear precision and infinite smoothness (Fig. 13).

In the following we are applying Warren's coordinates over an ADT with only convex elements for function and image interpolations from scattered values.

Fig. 12 Barycentric coordinate functions over ADT elements
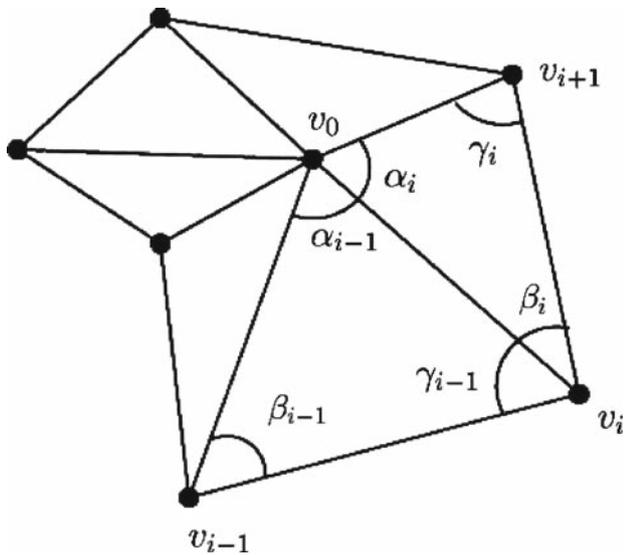
Fig. 13 Angles used in the definition of Mean Value Coordinates [9]

7 Interpolation applications

Franke's function [10] has been used as a benchmark in scattered data interpolation for a long time. We approximate this function by sampling its values at 40 to 400 arbitrary

locations in the unit square. The corresponding ADT tessellations are plotted in Fig. 14, with polygons of valence greater than three depicted in darker colors. The corresponding approximations of Franke's function are shown in Fig. 15. We remark that the scheme renders good results, even for low resolutions.

We also apply the ADT interpolation scheme on an 8 bit, 720×560 pixels grayscale image of Antonio Canova's "Eros and Psyche", shown in Fig. 16.

We consider as known the values in 4,292 pixels out of 403,200 (respectively 1.06%) and interpolate the values in the others. Two approaches are compared, namely a Delaunay triangulation with a linear interpolation over the simplices and an Adaptive Delaunay Tessellation with Warren's generalized barycentric coordinates over the polygons.

While the DT is a triangulation of the initial scattered point distribution, the ADT is also formed of polygons up to octagons (Fig. 17). The ADT partition contains 32% less elements compared to the DT one in this case. The interpolated pictures are presented in Figs. 18 and 19.

We compare the interpolation error for the two methods based on the common measures of root mean-square (RMS) error and relative absolute error. The RMS value was obtained by computing the average of squared differences between

Fig. 14 Two ADT tessellations over a unit square
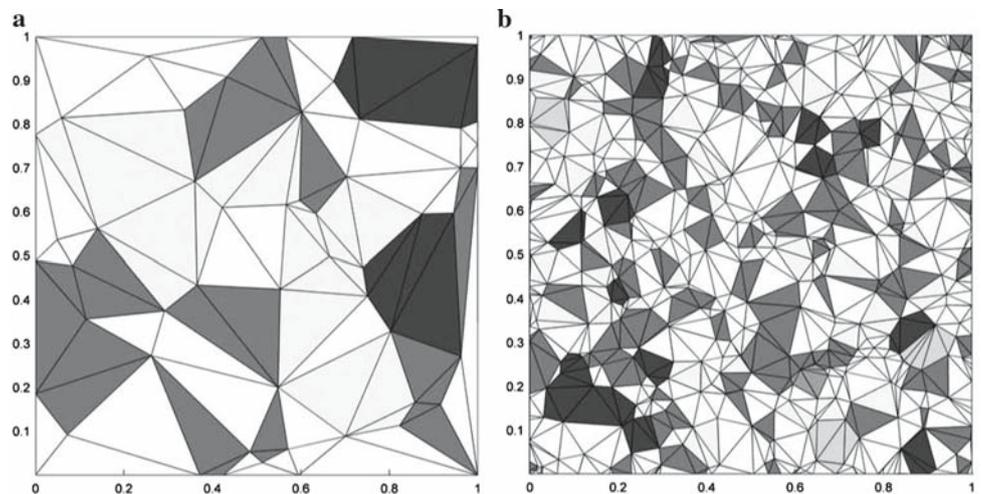
Fig. 15 Franke's function approximations
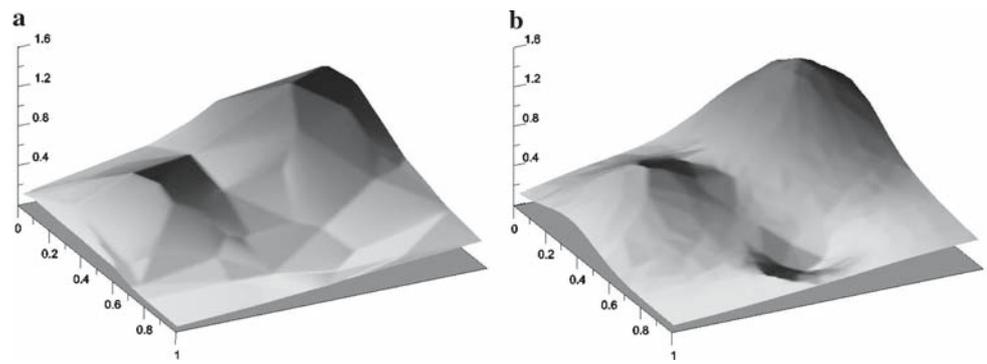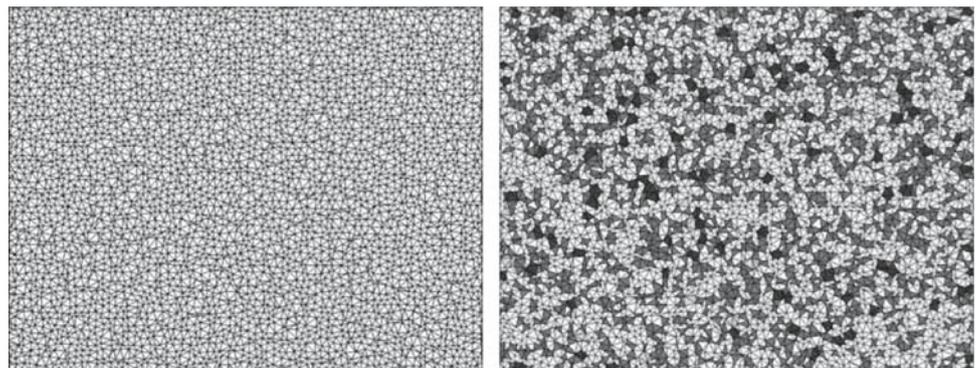

Fig. 16 Eight bit grayscale image

computed values c_i and true values t_i for all n test cases

$$\sqrt{\frac{[t_1 - c_1]^2 + \cdots + [t_n - c_n]^2}{n}}$$

We took $\bar{t}$ as the average of the true values and computed the relative absolute error value as

$$\frac{|t_1 - c_1| + \cdots + |t_n - c_n|}{|t_1 - \bar{t}| + \cdots + |t_n - \bar{t}|}.$$

The RMS value for the previously interpolated image was 4.5401 for the DT and 4.5619 for the ADT scheme. The relative absolute errors were 0.1659 and 0.1661 for the DT and the ADT scheme, respectively.

Despite using significantly fewer elements than a DT approach, the ADT scheme yields a similar interpolation error. From a visual point of view the interpolated image will be smoother, more obvious on tilings with few elements.

8 Galerkin application in two dimensions

### 8.1 Numerical integration

Gauss integration is largely used in finite elements and in most of the mesh-free Galerkin methods, where background integration cells are approximating the shape function's support. Yet, for non-polynomial coordinates, no Gaussian quadrature can guarantee an exact result. Moreover, due to the nodal character of our approach where representative areas around the nodes are computed at the meshing stage, evaluating the weak form via nodal integration becomes a natural alternative.

Traditionally, direct nodal integration has been altered by spurious (near-singular) modes and several different techniques have been applied for stabilization. We are using a recent stabilized conforming nodal integration approach

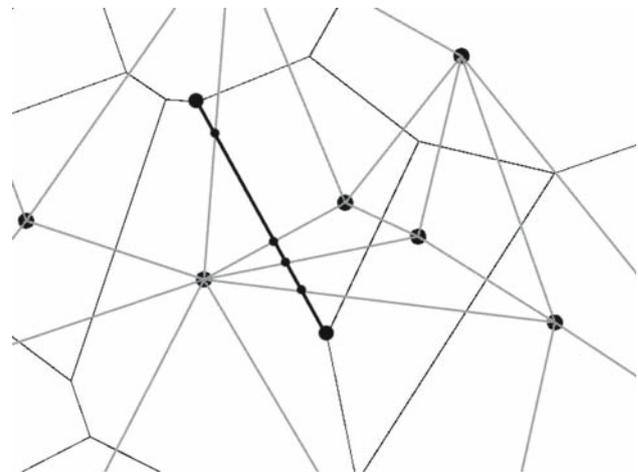**Fig. 17** Delaunay triangulation versus Adaptive Delaunay Tessellation

Fig. 18 DT interpolated image versus ADT interpolated image
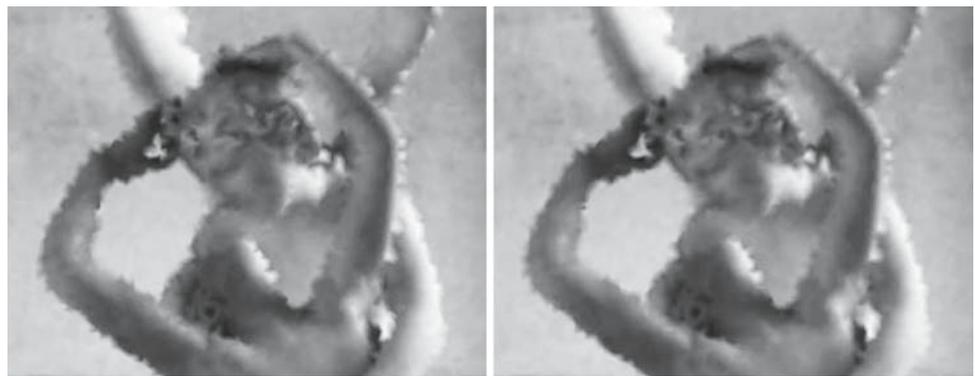
Fig. 19 DT versus ADT interpolated image (396 × 312 pixels detail)
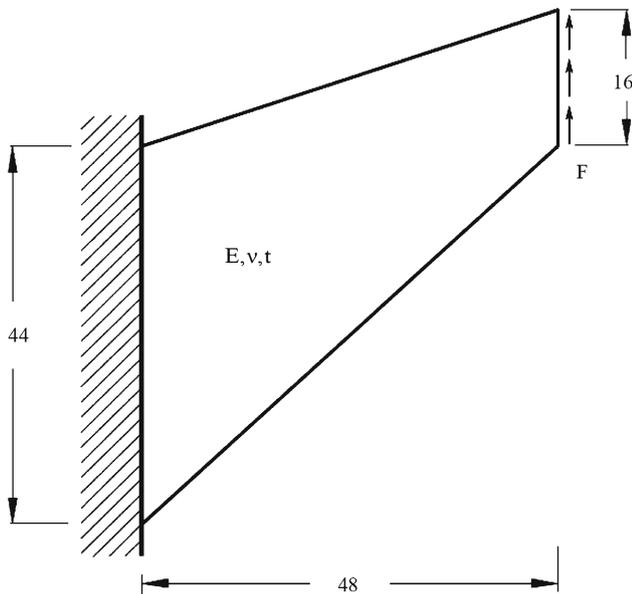
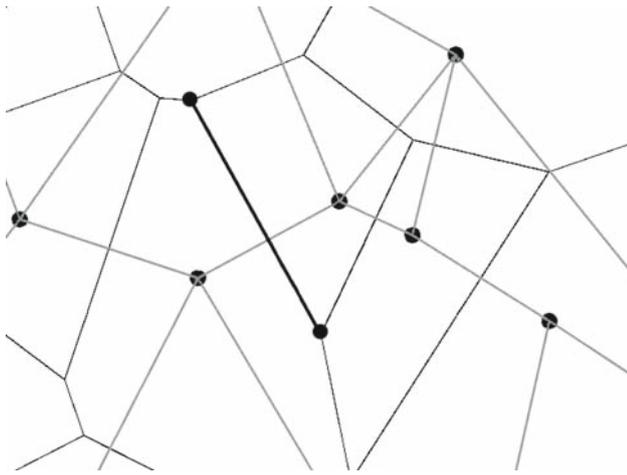**Fig. 20** Cook's membrane

Fig. 21 Linear coordinates on Delaunay simplices

which avoids instabilities generated by the vanishing derivatives of the shape functions at the nodes [4].

In this approach, the area integral of the derivative of shape function is replaced by a line integral of the shape function along the boundary of the voronoi tile of the nodes. This integral is represented by a linear combination of the values at the nodes that govern the underlying shape functions. Since for arbitrary shape functions, an analytic integration is not feasible, quadrature is used. It is however necessary to properly sample the Voronoi boundaries in order to cover all the shape functions that influence the integral. Depending on the underlying shape functions and/or tessellation, this integration requires different minimum step size and therefore a different amount of function evaluations. Computing the stiffness matrix entirely at the nodes proves to be an effi-

Fig. 22 Generalized barycentric coordinates on ADT elements

cient solution in our case, since the Voronoi cells are a priori known.

8.2 Cook's membrane problem

A linear elastic analysis of the classical Cook's membrane (Fig. 20) was performed under plane stress conditions ($F = 1$, $E = 1$, $t = 1$, $\nu = 0.3$).

Several samplings (with a different step size) of the Voronoi edges have been perfomed for the comparative study of accuracy of different interpolation schemes on Delaunay and ADT tessellations. The amount of shape function evaluations needed to properly compute the nodal stiffnesses was different in each case.

Firstly we have used linear shape functions on Delaunay simplices (Fig. 21). Since the end points of a Voronoi edge might be in non-adjacent triangles, extra care should be taken to include all the triangles that contain the edge. Therefore we need to evaluate the shape function in every triangle if we want to avoid singular stiffness matrices. Inside each triangle the shape function is linear, thus the trapezoidal rule with evaluations at the intersections with triangle edges is exact.

Secondly we have used generalized barycentric shape functions on ADT elements (Fig. 22). Since the whole Voronoi edge is covered by at most two ADT elements, we can apply the trapezoidal rule to the whole segment without missing any contribution. This approximation is faster in terms of number of evaluations.

We have also compared the two former approaches with natural neighbor shape functions on point clouds. Like above, the support of natural neighbor shape functions covers the Voronoi segments and therefore the same argument applies.

The results for the absolute difference between the vertical displacement value $u_y(P)$ at node P(48, 52) and a reference value obtained for 32,748 degrees of freedom are summarized in Fig. 23. Several scattered nodal distributions have been used ranging from 22 to 300 nodes. For every resolution, the final values have been averaged from 25 different computations.

Similar results for the stress values $\sigma_x(M)$ at node M(24, 52) are presented in Fig. 24.

As expected, the results are more consistent for the primary variables computations. The errors induced by obtaining the secondary variables, in a nodal or element-based approach, are not the main issue of this comparison.
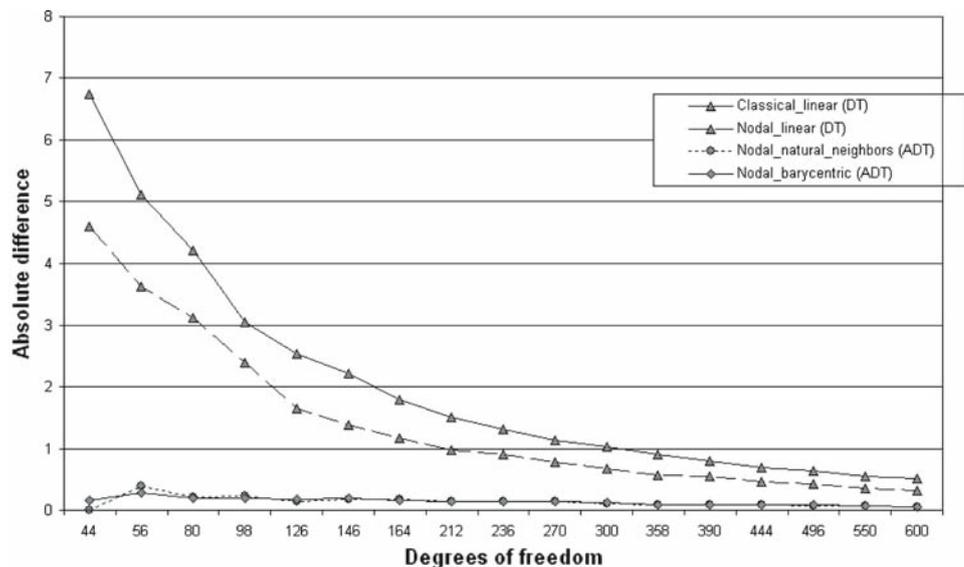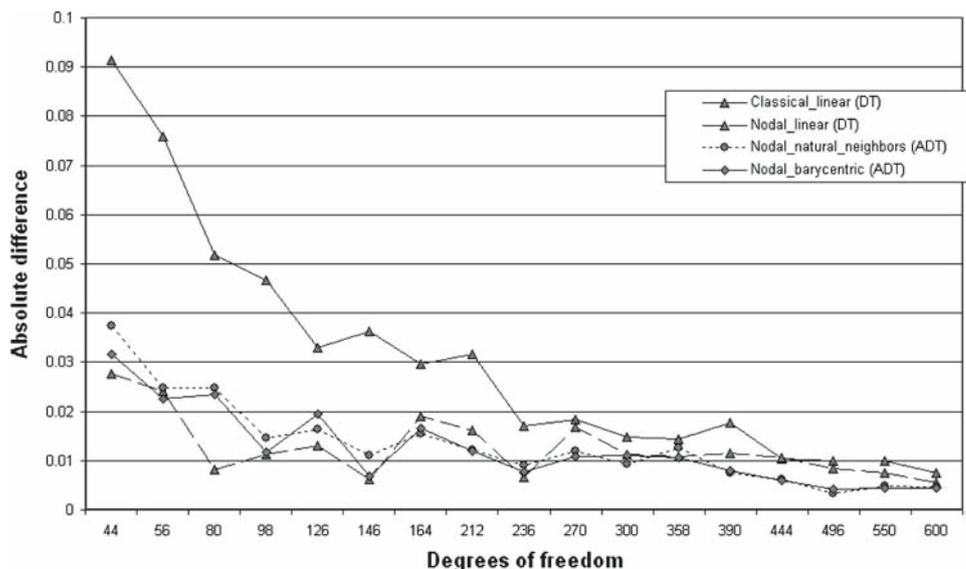
Fig. 23 Vertical displacement comparison

Fig. 24 Stress comparison

We remark that the results obtained with generalized barycentric coordinates on ADT elements are comparable with the ones obtained with natural neighbor interpolants on clouds of points. The superior geometrical qualities of the ADT elements versus Delaunay simplices and their better adaptivity to a scattered point distribution prove to be essential at lower resolutions. The computational convenience of an ADT mesh is a plus, expected to pay-off in higher dimensions.

9 Conclusions

A novel hybrid meshing technique has been proposed, and has been compared with the popular Delaunay tessellation when applied to scattered nodal distributions. The main advantages of the new scheme are its uniqueness, the bounded computational time and the improved geometrical qualities of its elements versus Delaunay simplices. The element condition number introduced is vital to the comparison in that it characterizes triangles as well as simple polygons. Furthermore, an ADT mesh is optimally adapted to scattered point distributions in the sense that the Voronoi cell of each point is entirely covered by its neighboring ADT elements. There exist easy to compute basis functions for arbitrary convex polytopes making the ADT an interesting approach both for scattered data interpolations and for numerical methods applications.

References

1. Aurenhammer F, Klein R (2000) Voronoi diagrams. Handb Comput Geom 5:201–290
2. Belikov V, Ivanov V, Kontorovich V, Korytnik S, Semenov A (1997) The Non-Sibsonian interpolation: a new method of interpolation of the values of a function on an arbitrary set of points. Comput Math Math Phys 37(1):9–15
3. Calvo N, Idelsohn SR, Onate E (2003) The extended Delaunay tessellation. Eng Comput 20(5/6):583–600
4. Chen JS, Wu CT, Yoon S, You Y (2001) A stabilized conforming nodal integration for galerkin mesh-free methods. Int J Numer Methods Eng 50:435–466
5. Delaunay B (1934) Sur la sphére vide. A la memoire de Georges Voronoi. Izv Akad Nauk SSSR, Otdelenie Matematicheskih i Estestvennyh Nauk 7:793–800
6. Descartes R (1644) La disposition de la matiere dans le systeme solaire et ses environs
7. Dirichlet GL (1850) Über die Reduktion der positiven quadratischen Formen mit drei unbestimmten ganzen Zahlen. Journal für die Reine und Angewandte Mathematik 40:209–227
8. Dyken C, Floater MS (2006) Preferred directions for resolving the non-uniqueness of delaunay triangulations. Comput Geom Theory Appl 43:96–101
9. Floater M (2003) Mean value coordinates. Comput Aided Geom Des 20:19–27
10. Franke R, Nielson G (1980) Smooth interpolation of large sets of scattered data. J Numer Methods Eng 15:1691–1704
11. Lawson CL (1977) Software for c^1 surface interpolation. Mathematical Software III pp 161–194
12. Sambridge M, Braun J, McQueen H (1995) Geophysical parameterization and interpolation of irregular data using natural neighbors. Geophys J Int 122:837–857
13. Shewchuk JR (1999) Lecture notes on Delaunay mesh generation. Department of Electrical Engineering and Computer Science, University of California at Berkeley
14. Shewchuk JR (2002) What is a good linear element? Interpolation, conditioning, and quality measures. Proceedings, 11th International Meshing Roundtable, pp 115–126
15. Sibson R (1978) A vector identity for the dirichlet tessellation. Comput J 21:243–245

16. Sibson R (1981) A brief description of natural neighbor interpolation. In: Barnett V (ed) Interpreting multivariate data. Wiley, NY, pp 21–36
17. Sukumar N (1998) The natural element method in solid mechanics, Ph.D. Thesis, Theoretical and applied mechanics, Northwestern University
18. Sukumar N, Malsch E (2006) Recent advances in the construction of polygonal finite element interpolants. Arch Comput Methods Eng 13:129–163
19. Sukumar N, Tabarraei A (2004) Conforming polygonal finite elements. Int J Numer Methods Eng 61:2045–2066
20. Voronoi G (1908) Nouvelles applications des paramétres continus á la théorie des formes quadratiques. Journal für die Reine und Angewandte Mathematik 133:97–178
21. Warren J, Schaefer S, Hirani A, Desbrun M (2003) Barycentric coordinates for convex sets. Tech. rep. Rice University, Houston
22. Watson DF (1981) Computing the n-dimensional Delaunay tessellation with application to Voronoi polytopes. Comput J 24(2): 167–172